A Multi-Objective Path Optimization Method for Plant Protection Robots based on Improved A*-IWOA (#103774)

First submission

Guidance from your Editor

Please submit by **10 Sep 2024** for the benefit of the authors (and your token reward) .

Structure and Criteria
Please read the 'Structure and Criteria' page for guidance.

Raw data check
Review the raw data.

Image check
Check that figures and images have not been inappropriately manipulated.

If this article is published your review will be made public. You can choose whether to sign your review. If uploading a PDF please remove any identifiable information (if you want to remain anonymous).

Files
Download and review all files from the materials page.

14 Figure file(s)
6 Table file(s)

Structure and Criteria

Structure your review

The review form is divided into 5 sections. Please consider these when composing your review:

1. **BASIC REPORTING**
2. **EXPERIMENTAL DESIGN**
3. **VALIDITY OF THE FINDINGS**
4. General comments
5. Confidential notes to the editor

You can also annotate this PDF and upload it as part of your review

When ready submit online.

Editorial Criteria

Use these criteria points to structure your review. The full detailed editorial criteria is on your guidance page.

BASIC REPORTING

- Clear, unambiguous, professional English language used throughout.
- Intro & background to show context. Literature well referenced & relevant.
- Structure conforms to PeerJ standards, discipline norm, or improved for clarity.
- Figures are relevant, high quality, well labelled & described.
- Raw data supplied (see PeerJ policy).

EXPERIMENTAL DESIGN

- Original primary research within Scope of the journal.
- Research question well defined, relevant & meaningful. It is stated how the research fills an identified knowledge gap.
- Rigorous investigation performed to a high technical & ethical standard.
- Methods described with sufficient detail & information to replicate.

VALIDITY OF THE FINDINGS

- **Impact and novelty is not assessed.** Meaningful replication encouraged where rationale & benefit to literature is clearly stated.
- All underlying data have been provided; they are robust, statistically sound, & controlled.
- Conclusions are well stated, linked to original research question & limited to supporting results.

Standout reviewing tips

The best reviewers use these techniques

Tip	*Example*
Support criticisms with evidence from the text or from other sources	*Smith et al (J of Methodology, 2005, V3, pp 123) have shown that the analysis you use in Lines 241-250 is not the most appropriate for this situation. Please explain why you used this method.*
Give specific suggestions on how to improve the manuscript	*Your introduction needs more detail. I suggest that you improve the description at lines 57- 86 to provide more justification for your study (specifically, you should expand upon the knowledge gap being filled).*
Comment on language and grammar issues	*The English language should be improved to ensure that an international audience can clearly understand your text. Some examples where the language could be improved include lines 23, 77, 121, 128 – the current phrasing makes comprehension difficult. I suggest you have a colleague who is proficient in English and familiar with the subject matter review your manuscript, or contact a professional editing service.*
Organize by importance of the issues, and number your points	*1. Your most important issue* *2. The next most important item* *3. …* *4. The least important points*
Please provide constructive criticism, and avoid personal opinions	*I thank you for providing the raw data, however your supplemental files need more descriptive metadata identifiers to be useful to future readers. Although your results are compelling, the data analysis should be improved in the following ways: AA, BB, CC*
Comment on strengths (as well as weaknesses) of the manuscript	*I commend the authors for their extensive data set, compiled over many years of detailed fieldwork. In addition, the manuscript is clearly written in professional, unambiguous language. If there is a weakness, it is in the statistical analysis (as I have noted above) which should be improved upon before Acceptance.*

A Multi-Objective Path Optimization Method for Plant Protection Robots based on Improved A*-IWOA

Jing Niu Corresp., Equal first author, 1 , **Chuanyan Shen** Equal first author, 1 , **Lipeng Zhang** 2 , **Qijun Li** 1 , **Haohao Ma** 1, 3

1 School of Mechatronics and Automotive Engineering, Tianshui Normal University, Tianshui, China

2 School of Vehicle and Energy, Yanshan University, Qinhuangdao, China

3 Department of Mechanical and Manufacturing Engineering, University Putra Malaysia, Serdang, Malaysia

Corresponding Author: Jing Niu
Email address: sensily@163.com

The energy consumption of pure electric-driven plant protection robots in mountainous environments has significantly increased, seriously affecting the efficiency of their operations. To address this issue, this paper proposes a multi-objective improved A*-IWOA robot path optimization method based on a 2.5D elevation grid map. Firstly, a work energy consumption model considering robot slope energy consumption is established based on robot kinematics and dynamics models. Then, based on a 2.5D elevation grid map, an improved A* search method is established by searching for 8-domain diagonal distances and introducing a cost function with cross product decision values. Then, with the robot's motion trajectory as the constraint condition, the IWOA algorithm with dynamically adjusted uniformly distributed population position and inertia weight is adopted to optimize the vector cross product factor p with the goal of minimizing the operation’s energy consumption and path curvature. Finally, in simulation and real mountainous orchard scenarios, the application effects of the improved algorithm in this paper are compared with some excellent variants of the A* algorithm using the robot ROS2 operating system as a platform. The experimental results show that this improved algorithm described here could significantly shorten the passage length of the robot, and improve the path planning effect and computational efficiency. This method largely meets the requirements for driving accuracy and energy consumption of plant protection robots in mountainous operation scenarios.

A Multi-Objective Path Optimization Method for Plant Protection Robots based on Improved A*-IWOA

Jing Niu[1], Chuanyan Shen[1], Lipeng Zhang [2], Qijun Li[1], Haohao Ma[1,3]
[1] School of Mechatronics and Automotive Engineering, Tianshui Normal University, Tianshui, China
[2] School of Vehicle and Energy, Yanshan University, Qinhuangdao, China
[3] Department of Mechanical and Manufacturing Engineering, University Putra Malaysia, Serdang, Malaysia
Corresponding Author:
Jing Niu[1]
Tianshui Normal University, Tianshui, Gansu, 741001, China
Email address: sensily@163.com

Abstract

The energy consumption of pure electric-driven plant protection robots in mountainous environments has significantly increased, seriously affecting the efficiency of their operations. To address this issue, this paper proposes a multi-objective improved A*-IWOA robot path optimization method based on a 2.5D elevation grid map. Firstly, a work energy consumption model considering robot slope energy consumption is established based on robot kinematics and dynamics models. Then, based on a 2.5D elevation grid map, an improved A* search method is established by searching for 8-domain diagonal distances and introducing a cost function with cross product decision values. Then, with the robot's motion trajectory as the constraint condition, the IWOA algorithm with dynamically adjusted uniformly distributed population position and inertia weight is adopted to optimize the vector cross product factor p with the goal of minimizing the operation's energy consumption and path curvature. Finally, in simulation and real mountainous orchard scenarios, the application effects of the improved algorithm in this paper are compared with some excellent variants of the A* algorithm using the robot ROS2 operating system as a platform. The experimental results show that this improved algorithm described here could significantly shorten the passage length of the robot, and improve the path planning effect and computational efficiency. This method largely meets the requirements for driving accuracy and energy consumption of plant protection robots in mountainous operation scenarios.

Keywords: Plant Protection Robots, Path Planning, Multi-Objective, Improved A*-IWOA, Vector Cross Product Winning Value

1 Introduction

The widespread application of agricultural robots has achieved deep integration of intelligent technology and agricultural machinery, greatly improving agricultural production efficiency and significantly reducing the labor intensity of farmers. Autonomous plant protection robots are widely used in farmland and orchards, and how to improve their operational accuracy, efficiency, and energy consumption is currently an important issue.

Autonomous operation and obstacle avoidance path planning are key technologies for plant protection robots. Plant protection robots provide reliable data for the rational planning of obstacle avoidance paths by sensing, detecting, and identifying obstacles through their own sensors. Farmland and orchards are typical unstructured scenes with characteristics such as uneven ground and a complex distribution of obstacles, which increase the difficulty of path planning. Li W et al. (2021) and SoundraPandian and Mathur (2010) have combined the A* algorithm with the DWA algorithm to obtain fewer path distances and inflection points. SoundraPandian and Mathur (2010) have moved the path points away from obstacles and used mixed A* to replan the path, improving the safe distance. Chen Y et al. (2023) have selected dynamic points on the line connecting the robot to the target point as feature vectors and planned to run the COA algorithm once per step until the target point was reached. Yuan Y et al. have proposed a combination matrix that combines energy consumption models and motion distances and applied it to the Dijkstra algorithm for path planning (Yuan et al., 2020; Wang D, 2012; Meng et al., 2023). An ECA* algorithm has been proposed that considers energy consumption constraints to solve the optimal energy consumption path planning problem in resource-limited situations (Zhai, Egerstedt & Zhou, 2022; Manca, Paternò & Santoro, 2021). Zakharov K et al. have proposed an LRLHD-A* algorithm for optimal path planning of robot energy consumption in three-dimensional map environments (Zakharov Saveliev & Sivchenko, 2020). The dynamic constraints during robot motion and their interaction with terrain are extremely complex, and the energy consumption model constructed by traditional methods has low accuracy. Lambert et al. (2024) have used a small amount of terrain perception data to train and generate more accurate energy consumption models through deep meta-learning algorithms.

From the above analysis, it can be concluded that the two key factors to consider in the path optimization process of plant protection robots are energy consumption and path optimization, which in turn affect each other. The length and smoothness of the path will both affect energy consumption. In our study, based on a 2.5-dimensional elevation grid map, a work energy consumption model considering the additional energy consumption of robot slopes is established, and an improved A *-IWOA path planning algorithm is designed with the kinematic constraints of robot motion trajectory as the boundary condition, ensuring a good balance between energy consumption and trajectory smoothness in the robot's work effect.

2 Kinematic and energy consumption models of the plant protection robot

This research object is a front wheel differential driven Ackermann steering plant protection robot working in unstructured orchard scenes. This robot coordinate system XYZ is defined in the geodetic coordinate system $X_0Y_0Z_0$, where the X-axis points directly in front of the robot's operation, the Y-axis points forward towards the left side of the robot, and the Z-axis is perpendicular to the robot's moving platform, as shown in Fig. 1. Considering the influence of the robot's operational status and orchard terrain factors, the kinematic state space equations is established in this article for the movements in the three directions along X-axis, Y-axis, and Z-axis and the lateral motion around the Z-axis.

2.1 Kinematic model

This robot motion state variable is defined as $X = [v_x, \omega]$, where v_x is the velocity component along the X-axis and ω is the lateral angular velocity around the z-axis. $U = [\omega_l, \omega_r]$ is defined as control variables, where ω_l and ω_r respectively represent the angular velocity of the left and right drive wheels of the robot. The motion state equation of the robot could be expressed as:

$$\begin{bmatrix} v_x \\ \omega \end{bmatrix} = \frac{r}{B} \begin{bmatrix} \frac{B}{2} & \frac{B}{2} \\ -1 & 1 \end{bmatrix} \begin{bmatrix} \omega_l \\ \omega_r \end{bmatrix} \tag{1}$$

$$z = \sigma \tag{2}$$

Where: r is the radius of the robot wheel. B is the robot track width. Z is the z-axis displacement of the robot. σ is the road elevation.

The kinematic model of this robot is represented by its unilateral driving wheel motion state as (Zhang et al., 2023):

$$\mathbf{M}\ddot{\boldsymbol{\theta}} + \mathbf{C}(\boldsymbol{\theta}, \dot{\boldsymbol{\theta}}) + \mathbf{G}(\boldsymbol{\theta}) = \mathbf{T} \tag{3}$$

Among them: $\boldsymbol{\theta} = [\theta_l, \theta_r]$, $\dot{\boldsymbol{\theta}} = [\omega_l, \omega_r]$, $\mathbf{T} = [T_l, T_r]$.

Where: M is the inertia matrix of the robot's driving wheel. $\mathbf{C}(\boldsymbol{\theta}, \dot{\boldsymbol{\theta}})$ is the matrix of the ground rolling resistance moment of the driving wheel. $\mathbf{G}(\boldsymbol{\theta})$ is the gravity matrix of the robot. $\boldsymbol{\theta}$ is the angular displacement vector of the left and right driving wheels of the robot. $\dot{\boldsymbol{\theta}}$ is the angular velocity vector of the left and right driving wheels of the robot. $\ddot{\boldsymbol{\theta}}$ is the angular acceleration vector for the left and right driving wheels of the robot. $\mathbf{T}$ is the output torque matrix for the motor of the left and right drive wheels.

The correspondence between the robot control variable U and the output torque vector T of the driving wheel can be obtained through formulas (1) to (3), laying the foundation for the establishment of its energy consumption model.

2.2 Energy consumption model

This pure E-driven plant protection robot uses power batteries as the power source, and the motor controller achieves speed control of the driving motor through PWM (Modulation and

Demodulation) methods. A portion of the power output from the driving motor is used to consume the internal resistance of the battery, while the other portion is output to the robot's moving platform.

The movement speed of the plant protection robot is relatively small, and the tire contact area is limited, so the air resistance and rolling resistance could be ignored. But the terrain of the orchard is undulating, and the total mass of the robot is relatively large, so the ramp resistance could not be ignored (Yin et al., 2019). Therefore, this paper defines that the energy consumption of operations consists of two parts, namely battery internal resistance loss and robot ramp resistance loss.

When the robot load and the motor output torque are constant, according to the direct proportional relationship between motor torque and armature current, it can be inferred that both I_l and I_r are constant values. The armature voltage of the left and right drive motors could be expressed as:

$$U_l = I_l R_B + K_M i_0 \omega_l \tag{4}$$

$$U_r = I_r R_B + K_M i_0 \omega_r \tag{5}$$

Where: I_l and I_r are the armature currents of the left and right drive motors respectively. R_B is the internal resistance of the power batteries. U_l and U_r are the armature voltages of the left and right drive motors, respectively. K_M is the back electromotive force coefficient of the driving motor. i_0 is the transmission ratio of the motor reducer.

The output power of the left and right drive motors could be expressed as:

$$P_l = U_l I_l \tag{6}$$

$$P_r = U_r I_r \tag{7}$$

Substituting formulas (4) and (5) into formulas (6) and (7), it could be obtained as:

$$P_l = I_l^2 R_B + K_M i_0 \omega_l I_l \tag{8}$$

$$P_r = I_r^2 R_B + K_M i_0 \omega_r I_r \tag{9}$$

The internal resistance loss of the battery could be expressed as:

$$Q_B = (I_l^2 + I_r^2) R_B \sum_{i=1}^{N} \frac{ds_i}{v_x} \tag{10}$$

Where: N is the number of state nodes in the path search node space. ds_i is the distance between adjacent state nodes.

Assuming the longitudinal ramp angle of the road surface is α, the ramp resistance loss could be expressed as:

$$F_i = mgtan\alpha \tag{11}$$

$$tan\alpha = D \cdot \frac{z_{i+1} - z_i}{d_0}, \quad z_{i+1} \geq z_i \tag{12}$$

Where: m is the total mass of the robot, ignoring the changes in the mass during operation process. the value of coefficient D is related to the search logic, such as D=1 for straight line search and D=0 for diagonal search. d_0 is the distance between the centers of adjacent cells in a grid map.

So the ramp resistance loss could be expressed further as:

$$Q_i = \frac{mgD}{d_0} \sum_{i=1}^{N} (z_{i+1} - z_i) \frac{ds_i}{v_x} \tag{13}$$

By summing formulas (10) and (13), the energy consumption model of the robot can be obtained as:

$$Q = \sum_{i=1}^{N} [\mathrm{A} + \mathrm{B} \ \ (z_{i+1} - z_i)] \frac{ds_i}{v_x} \tag{14}$$

Where: A and B represent constant coefficients related to the robot structural parameters and node search logic respectively.

3 An improved A* path searching method based on the constraints of operation conditions

The A* algorithm is a heuristic searching method to find the optimal path in a static obstacle environment (Jiang & Zhang, 2022). It searches in the robot's motion state space. Firstly, it evaluates the cost of each search position to obtain the state node with the smallest cost. Then it traverses the entire state space until the optimal solution is found. At last, it ends the cycle.

In this heuristic search process, the cost evaluation of state nodes is very important. And their cost function is generally expressed as:

$$\mathrm{f(n)} = \mathrm{g(n)} + \mathrm{h(n)} \tag{15}$$

Where: f(n) is the cost function from the initial state through the state n to the target state. g(n) is the actual cost from the initial state to the state n in the state space. h (n) is the estimated cost of the optimal path from the state n to the target state.

There are three common h(n) functions in 2D grid maps, namely euclidean distance, Manhattan distance, and diagonal distance methods as shown in Fig. 2 (Min et al., 2021). The euclidean distance is the shortest among them, but it can lead to a decrease in search efficiency when the environmental map is more complex. The search logic for Manhattan distance is simple, but the path distance is longer. In contrast, the diagonal distance method performs better in both search path distance and search efficiency (Shi et al., 2022).

3.1 The improvement of A^* based on the cost function of vector cross product winning value

In this paper, it is considered that the limitations of 2D grid information in describing the working environment and the high demand for computing resources in the 3D occupied grid map of the octree structure (Wu et al., 2022). In addition, based on the analysis above, energy consumption in mountainous environments is also a factor that cannot be ignored in path selection. Therefore, a 2.5D elevation grid map is selected to describe the robot's working environment accurately, as shown in Fig. 3. In Fig. 3(b), the numbers in each grid represent the vertical height from the horizontal plane at the center point of the divided grid, denoted as z_n. This can ensure efficient representation of environmental information while also having lower maintenance costs and real-time performance (Kim & Kim, 2024). We can see that the planned path obtained in a 2.5D elevation grid map is completely different from the 2D grid environment without considering the vertical height of the mountains in the simulation results in Section 5.3 of this paper.

According to the 8-domain diagonal distance search method (Saadatzadeh, Ali Abbaspour & Chehreghan, 2023), a cost function with a cross product winning value is introduced to make the planned path more inclined to follow the straight path from the initial point to the target point (Bays et al., 2024), as shown in Fig. 4. The specific definition is as follows:

$$dx1 = x_n - x_{goal} \tag{16}$$

$$dy1 = y_n - y_{goal} \tag{17}$$

$$dz1 = z_n - z_{goal} \tag{18}$$

$$dx2 = x_{start} - x_{goal} \tag{19}$$

$$dy2 = y_{start} - y_{goal} \tag{20}$$

$$dz2 = z_{start} - z_{goal} \tag{21}$$

In the following, **u** and **v** represent the vector from the current point to the target point and the vector from the starting point to the target point, respectively:

$$\mathbf{u} = (dx1, dy1, dz1) \tag{22}$$

$$\mathbf{v} = (dx2, dy2, dz2) \tag{23}$$

To measure the deviation of the planned straight path between the current node and the starting and target points, the cross product vector of **u** and **v** is defined as follows:

$$\mathbf{u} \times \mathbf{v} = \begin{bmatrix} i & j & k \\ dx1 & dy1 & dz1 \\ dx2 & dy2 & dz2 \end{bmatrix} = (dy1 * dz2 - dy2 * dz1, dz1 * dx2 - dx1 * dz2, dx1 * dy2 - dy1 * dx2)$$

(24)

On this basis, define the vector cross product winning value as follows:

$$cross = \sqrt[2]{(dy1 * dz2 - dy2 * dz1)^2 + (dz1 * dx2 - dx1 * dz2)^2 + (dx1 * dy2 - dy1 * dx2)^2}$$

(25)

Therefore, the cost function by introducing the vector cross product winning value is redefined as follows:

$$h(n) = 1 + cross * p \qquad (26)$$

Where: (x_n, y_n, z_n), $(x_{start}, y_{start}, z_{start})$, $(x_{goal}, y_{goal}, z_{goal})$ are the coordinates of the current state node, the starting point and the target point respectively. p is the vector cross product weight factor.

In Fig. 4, the parallelogram area composed of **u** and **v** vectors represents the value of the cross. The greater the deviation between the current path and the straight path from the starting point to the target point, the greater the value of this cross. According to the tendency of the cost function, the selection of path nodes tends to choose the direction closer to the straight path. In this case, when the p-value is selected properly and there are no obstacles, A^* can not only search for very few state regions, but also find excellent paths. Assuming p is chosen as a fixed value, when a large number of obstacles appear, A^* would produce strange results, as shown in Fig. 5 (Wang Wang & Liu, 2024). Therefore, in Section 3.2 below, the intelligent optimization algorithm WOA is adopted to intelligently optimize the vector cross product factor p with the goal of minimizing robot operation energy consumption and path curvature.

3.2 Constraints of operation trajectory

As shown in Fig. 6, the operation trajectory of the plant protection robot is divided into straight and curved segments. The search logic of the straight section is simple and will not be repeated in the text. The points Q_0~Q_6 in the figure represent seven consecutive state nodes in the search space of a certain curve segment trajectory, where Q_0 (x_0, y_0) and Q_6 (x_6, y_6) are the starting and target points, respectively. Q_1 (x_1, y_1) and Q_5 (x_5, y_5) are the segmentation points. To simplify the turning logic trajectory, it is symmetrically distributed along the center line. Therefore, changing the positions of Q_2 (x_2, y_2) and Q_4 (x_4, y_4) could improve the smoothness of the trajectory. Due to the special working environment and structural parameter limitations of robots, the following requirements are proposed for the motion trajectory in the path planning process:

(1) The curvature of any point on the trajectory $\rho \leq \frac{1}{R_{min}}$, where R_{min} is the minimum turning radius of the robot.

(2) Front wheel turning angle of the robot $\delta \leq \delta_{max}$, where $\delta_{max} = \arctan\frac{L}{R_{min}}$.

(3) The trajectory curvature must be continuous. To avoid situations such as sharp turns and emergency stops during the operation, it is necessary to ensure the curvature of the trajectory is continuous. Therefore, the point Q_2 should be located above the line connecting Q_1 and Q_3, otherwise the trajectory curvature changes too much, which is not conducive to tracking (Zhai et al., 2024). Ignoring the influence of smaller elevation parameters in a 2.5-D elevation grid map, the curvature continuity condition can be expressed as:

$$y_2 \geq \frac{y_3 - y_1}{x_3 - x_1}(x_2 - x_1) + y_1 \tag{27}$$

(4)The angular velocity constraints of robot front wheel :

$$\frac{d\delta}{dt} = \frac{d(arctan\frac{2Lsin\varphi}{l_d})}{dt} \leq \omega_{max} \tag{28}$$

This paper uses cubic B-spline curves to fit trajectories (Ardestani, Safdari & Mallah 2023), and the above trajectory constraints can be summarized as follows:

$$\begin{cases} \rho(t) = \dfrac{y'(\boldsymbol{u})x''(\boldsymbol{u}) - x'(\boldsymbol{u})y''(\boldsymbol{u})}{(x'^2(\boldsymbol{u}) + y'^2(\boldsymbol{u}) + z'^2(\boldsymbol{u}))^{\frac{3}{2}}} \leq \dfrac{1}{R_{min}} \\ y_2 \geq \dfrac{y_3 - y_1}{x_3 - x_1}(x_2 - x_1) + y_1 \\ \dfrac{d(arctan\frac{2Lsin\varphi}{l_d})}{dt} \leq \omega_{max} \end{cases} \tag{29}$$

Where: $\boldsymbol{u}$ is the node vector of the cubic B-spline curve. l_d is the forward viewing distance of the robot. φ is the heading angle between the current position of the robot and the target point.

4 Multi-objective optimization of the vector cross product weight factors

4.1 A brief introduction to WOA

The WOA algorithm is a meta-heuristic algorithm that simulates the hunting behavior of humpback whales in the ocean. It simulates the three stages of whale hunting, such as searching for prey, surrounding targets, and spiral bubble net predation. Compared to the other intelligent algorithms, it has the advantages of fewer parameters, simpler principles, and stronger multi-objective optimization ability (Guo et al., 2021). The three stages of whale hunting can be described by mathematical models as follows (Rahimnejad, Akbari & Mirjalili, 2023):

(1)The surrounding preys stage. Other whale individuals in the population use formulas (30) to (34) to update their positions and approach to the optimal whale individual.

$$X_i^{t+1} = X_{best}^{t} - A \cdot D_1 \quad (30)$$

$$D_1 = \left| C \cdot X_{best}^{t} - X_i^t \right| \quad (31)$$

$$A = 2a \cdot r - a \quad (32)$$

$$C = 2 \cdot r \quad (33)$$

$$a = 2 - 2\frac{t}{T} \quad (34)$$

Where: X_{best}^{t} is the location of the whale individual that searched for the optimal solution of the t-th generation population. X_i^t is the position of the i-th individual in the t-th iteration. D_1 indicates the enclosing step size. A and C are the coefficient vectors. T is the maximum number of iterations. r is a random number between [0, 1].

(2)The bubble net attack stage. It simulates the process of whales protruding the bubble net along the spiral line and approaching their preys using formulas (35) to update individual positions:

$$X_i^{t+1} = D_2 \cdot e^{bl} \cdot cos(2\pi l) + X_{best}^{t} \quad (35)$$

Where: $D_2 = \left| X_{best}^{t} - X_i^t \right|$ expressthe distance between whales and prey;b is the spiral shape coefficient; l is a random number between [0,1].

(3)The searching for prey stage. WOA selects an individual from the population as the target for position updates randomly, and updates the model as shown in equation (36),

$$X_i^{t+1} = \begin{cases} X_{rand}^{t} - A \cdot D_3, & p < 0.5; \\ D_2 \cdot e^{bl} \cdot cos(2\pi l) + X_{best}^{t}, & p \geq 0.5 \end{cases} \quad (36)$$

$$D_3 = \left| C \cdot X_{rand}^{t} - X_i^t \right| \quad (37)$$

Where: X_{rand}^{t} is a randomly selected individual position from the whale population.

4.2 Improvement of IWOA based on dynamic adjustment of uniformly distributed population position and inertia weights

When initializing the WOA algorithm population, randomly generated population positions can easily lead to an uneven distribution of individual positions, limited search range, slow convergence speed, and falling into local optima (Yang & Liu, 2022; Li et al., 2017). In response to the shortcomings of the aforementioned WOA algorithm, this paper uses Circle mapping to generate uniformly distributed population positions, increasing the diversity of whale individual positions and improving the performance of WOA (Zhou et al., 2017).

The definition of Circle mapping is as follows:

$$X_i^{t+1} = \mathrm{mod}(X_i^t + 0.2 - \frac{0.5}{2\pi}\sin(2\pi X_i^t),1) \quad (38)$$

Where: X_i^t represents the position vector of the i-th whale in the whale population at the t-th position update.

Dynamic adjustment for inertia weight of fitness ω based on Γ inverse incomplete function (Li, 2024), with the specific form as follows:

$$\omega = \frac{\omega_{max} - \omega_{min}}{\lambda} \times \mathrm{gammaincinc}(\lambda,1-\frac{t}{T}) \quad (39)$$

Where: $\omega_{max} = 0.8, \omega_{min} = 0.3$; $\mathrm{gammaincinc}(\lambda,a)$ is a MATLAB Γ function which is $\gamma(\lambda,a) = \int_0^\lambda e^{-t}t^{a-1}dt$; $\lambda(\lambda \geq 0)$ is a random variable with a value of 0.2. t is the current number of iterations. T is the maximum number of iterations. By dynamically adjusting, the inertia weight ω decreases non-linearly with the increase of iteration times. Based on this, the improved IWOA position update formula is as follows:

$$X_i^{t+1} = \begin{cases} \omega \cdot X_{best}^t - A \cdot D, & |A| < 1, p < 0.5; \\ \omega \cdot X_{rand}^t - A \cdot D_{rand}, & |A| \geq 1, p < 0.5 \\ D \cdot e^{bl} \cdot cos(2\pi l) + \omega \cdot X_{best}^t & ,p \geq 0.5 \end{cases} \quad (40)$$

Where: X_{rand}^t represents the position vector of whales randomly selected from the whale population in the t-th position updating. X_{best}^t represents the optimal whale position vector from the whale population in the t-th position updating. p represents the probability of choosing to reduce the enclosure and update the spiral rotation position during whale hunting. $D = |C \cdot X_{best}^t - X_i^t|$; $D_{rand} = |C \cdot X_{rand}^{*t} - X_i^t|$ (X_{rand}^{*t} represents the position vector of whales randomly selected from the population). b represents the constant of the spiral equation, is 1 in this paper. l is random numbers between [-1,1]. A and C are two random parameters, defined as follows:

$$A = 2ar_1 - a, \quad C = 2r_2 \quad (41)$$

Where: r_1 and r_2 are random numbers between [0, 1]. a is a parameter that decreases from 2 to 0 as the number of iterations increases, it defined as:

$$a = 2 - 2t/T \quad (42)$$

Perform the search steps following the pseudo code of the improved IWOA algorithm shown in Table 1.

4.3 Process of multi-objective IWOA based on optimal solution evaluation

The distance between any two adjacent state nodes in the robot path:

$$S_i = [(x_{i+1} - x_i)^2 + (y_{i+1} - y_i)^2 + (z_{i+1} - z_i)^2]^{\frac{1}{2}} \quad (43)$$

During the operation of the plant protection robot, the longitudinal speed change is relatively small and can be considered to have a certain value. Therefore, substituting formula (43) into (14) can obtain the energy consumption of the robot from the starting point to any point:

$$Q = \sum_{i=1}^{N} [A + B \ (z_{i+1} - z_i)] \frac{ds_i}{v_x} \quad (44)$$

Where: when $z_{i+1} \geq z_i$, $B \neq 0$; else $z_{i+1} < z_i$, $B = 0$.

The general parameter equation of the trajectory curve in three-dimensional space can be expressed as:

$$x = x(t), y = y(t), z = z(t) \quad (45)$$

The curvature of any point on the robot's operation path can be expressed as:

$$\rho(t) = \frac{y'(t)x''(t) - x'(t)y''(t)}{(x'^2(t) + y'^2(t) + z'^2(t))^{\frac{3}{2}}} \quad (46)$$

Therefore the two fitness functions are established of the IWOA algorithm, which are:

$$f_1(x_i, y_i, z_i) = Q, \quad f_2(x_i, y_i, z_i) = \rho(t) \quad (47)$$

This paper uses the search logic selected by the optimal solution evaluation to search for non inferior optimal solutions (Cai et al., 2024). By $f_1(x_i,y_i,z_i)$and$f_2(x_i,y_i,z_i)$jointly guiding the whale's position in the decision variable space, it can fall into the non-inferior optimal target domain. This logic of selecting this optimal solution evaluation can be explained as this updating logic could cause $f_1(x_i,y_i,z_i)$ and $f_2(x_i,y_i,z_i)$ to change in different directions that increase at the same time. Ultimately, the whale's position is dispersed in a set of non inferior optimal solutions, which can prevent individual whales from falling into the optimal solution region of a certain fitness function, reflecting the constraint relationship between the two fitness functions. The specific process is shown in Fig. 7.

5 Experiments and analysis

Our experimental subject is a wheeled plant protection robot independently developed by our university, as shown in Fig. 8. The visual sensor of this robot platform adopts the OBI Zhongguang global shutter binocular depth camera, which has a depth frame rate of 90 fps. The 16-line LiDAR uses the Raytheon M10P, with a measurement radius and sampling frequency of 30 m and 20000 Hz, respectively. The processor uses NVIDIA's Orin Nano NX 8 GB and is equipped with the Ubuntu 18.04 LTS operating system. The overall functional design is completed based on ROS 2. The operating speed of the robot platform is 2-5 km/h.

5.1 Experimental methods

In order to verify the robustness of the algorithm proposed in this paper and the improvement effect of path planning in typical job scenarios, the experiment is conducted in three parts. First, the improvement effect of the IWOA algorithm based on the dynamic adjustment of uniformly distributed population position and inertia weight in a simulation environment was compared with that of the Whale Optimization Algorithm (WOA), the Whale Optimization Algorithm (LWOA) using Levy aircraft to optimize and update position (Zhao & Peng, 2023), the Whale Optimization Algorithm (MWOA) based on probability selection (Niu, Zhai & Ji, 2024), the Whale Optimization Algorithm (HSWOA) introducing the hunger concept (Liang, Hong & Yu, 2023), the Whale Optimization Algorithm (CamWOA) using correction factors to reduce iteration step size (Saha et al., 2022), and the Whale Optimization Algorithm (WWOA) incorporating adaptive weights (Cheng et al., 2022). At the same time, 20 comparative experiments are conducted under six typical benchmark test functions to objectively reflect the robustness and effectiveness of the algorithm improvement through the average convergence curve of the fitness function. Secondly, in a simulation environment, six environmental maps with different starting points, target points, and the number and location of obstacles are selected as the testing scenarios for improving the A*-IWOA algorithm's path planning. The effectiveness of the algorithm was verified by comparing it with the traditional A* algorithm's path planning performance in terms of running time, running length, number of turning points, and energy consumption. Finally, to verify the effectiveness of the A*, standard A*-IWOA, and the improved A*-IWOA algorithms, a physical experiment is conducted in a mountainous orchard scene in Gansu.

5.2 Performance testing of improved IWOA algorithm

In this experiment, six commonly used benchmark test functions from the IEEE CEC benchmark test set are used, covering unimodal, multimodal, and composite functions, as shown in Table 2 (Huang et al., 2023). Set the population size to 30 and the maximum number of iterations to 500. Due to the fact that the dimension of an algorithm is an important factor affecting its optimization ability, the dimensions of the six test functions mentioned in Table 2 vary from 2 to 30 dimensions, which can more comprehensively test the algorithm's solving ability from low to high dimensions.

In Fig. 9, the average convergence curves of the fitness functions have been obtained by running 6 benchmark test functions 20 times each are shown. The f_1 and f_5 curves evaluate the algorithm's development ability (Figure 9(a-b)), the f_8 and f_{13} curves evaluate the algorithm's search ability (Figure 9(c-d)), and the f_{15} and f_{17} curves evaluate the algorithm's comprehensive ability (Figure 9(e-f)). It can be seen that, due to the introduction of Circle mapping for uniformly distributed population positions and inertia dynamic adjustment of weights, the algorithm is more prone to jumping out of local optima. The improved IWOA algorithm has better convergence speed and accuracy in solving unimodal, multimodal, and composite functions than other algorithms, reflecting the effectiveness of the improved algorithm.

Table 3 reflects the running results data of the above test functions, where the optimal value, worst value, and average value usually reflect the optimization ability and effectiveness of the algorithm, and the standard deviation reflects the stability of the algorithm. As shown in Table 3, when solving the unimodal function f_1, multiple indicators of improved IWOA reached their theoretical value of 0, and the time consumption was the shortest. When solving the multimodal function f_{13}, the improved IWOA significantly accelerates its convergence speed by 20% compared to other excellent variants of WOA algorithms. When solving the composite function f_{15}, the improved IWOA randomly calculates the changes in dimensions, and its multiple indicators also approached the theoretical value of 0.1484. Although the time consumption increased slightly, it is still the fastest among these algorithms. It can be seen that the optimization performance and time efficiency of the improved IWOA are significantly improved by dynamically adjusting the position and inertia weight of the uniformly distributed population using circle mapping.

5.3 Path planning testing in 2.5D elevation grid map simulation

This algorithm simulation experiment uses a Windows 10 system, 32 GB of running memory, a 2.9 GHz CPU, and a Matlab R2021b programming workstation. The kinematic parameters of this robot and the initial parameter settings of the improved A*-IWOA are shown in Tables 4 and 5, respectively. We use 20×20 and 30×30, these two kinds of grid maps, respectively. Each cell array represents the horizontal, vertical, and elevation values at the center point of the cell, respectively. In the simulation process, we use the hue H value in the HSV model (Ren et al., 2013) to represent the cell elevation value, and the greater the hue H value, the greater the elevation value. For example, the elevation value of a purple cell is greater than that of a red cell. According to the path search logic described in this paper, in the main search area of the path nodes, we use the method of randomly distributing cell elevation values for the simulation test (Akay B & Karaboga, 2010; Akyol & Alatas, 2020; Al-Dabbagh RD et al., 2014; Aragón, Esquivel & Coello, 2010). Here, six representative scenarios of plant protection robots are constructed. The A*, standard A*-IWOA, and improved A*-IWOA were used for path planning simulation testing, and the test results are shown in Fig. 10.

In Fig. 10(a)~(e), the occupancy rate of obstacles in the robot passage area is 20%. We use

20×20 grid maps in Fig. 10(a)~(d) and (f), respectively 30×30 grid maps in Fig. 10(e). The solid black lines represent the path planned by the A* algorithm. The red dotted lines represent the path planned by the standard A*-IWOA algorithm. The green dotted lines represent the path planned by the improved A*-IWOA algorithm. It can be seen that the improved A*-IWOA algorithm performs significantly better than the other two algorithms in terms of the number of turning points, the total distance of the path, and the search time. The relevant experimental results are shown in Table 6. In Fig. 10(e), according to the search logic of the 8-domain cross-product decision value adopted by the improved A*-IWOA, the search failed at the second node in the path search space. Therefore, from the test results, it can be seen that the improved A*-IWOA has certain limitations and requirements for application scenarios; that is, it is best not to have too many obstacles near the starting point of the path. Alternatively, it is not suitable to use grid maps that are too small in size. In Fig. 10(f), we increase the obstacle occupancy rate to 30%. The total distance, number of turning points, and search time planned by the improved A*-IWOA are reduced by an average of 26%, 40%, and 31% compared to the other two algorithms.

In order to provide a more realistic representation of the inter-row working environment of fruit trees in mountainous environments, we use a 10×10 2.5D elevation grid map, where black obstacles represent the inter-row positions of fruit trees and different colors of the grid distinguish the vertical heights of their positions. The green grid represents the starting position of the robot, and the yellow grid represents the target position of the robot. On the Matlab R2021b programming workstation, we test the path planning effect of improved A*-IWOA both using 2D and 2.5D maps, respectively. The experimental results are shown in Fig. 11. We can see that the paths planned by the two are completely different. In Fig. 11(b), due to the difference in vertical height of the road surface, robots tend to choose the direction of low-lying terrain to move forward.

5.4 Experiment on robot operation path planning in real orchard

To verify the effectiveness of the above-improved algorithm, a physical experiment is conducted in a mountainous orchard scene in Gansu, as shown in Fig. 12. In this orchard, the plant spacing is 20–30 cm, and the row spacing is 70–80 cm. By adjusting the camera and radar-ranging height of the plant protection robot, ensure that there are no less than five plants in the camera's field of view within the robot's speed limit range. The K-means clustering method is used to obtain the position of the main trunk of the fruit tree (as shown in Fig. 13), and the navigation line is planned by delineating the communicable area through the central area. By comparison, the variation within the width range of 70–80 cm has a relatively small impact on the recognition error of the central area. In this experiment, the maximum error of the navigation line is 7.07 cm, the minimum error is 0.5 cm, and the average error is 3.1 cm.

In the physical environment, the A*, standard A*-IWOA, and improved A*-IWOA algorithms are loaded onto the robot ROS2 platform, respectively, and the path planning effects obtained are shown in Fig. 14. In this figure, the improved A*-IWOA chose a more direct and non-detour path. On the contrary, the other two algorithms chose a longer path to detour outside the obstacles.

6 Conclusions

For the unstructured work scenario of plant protection robots in mountainous orchards, this paper proposes an 8-domain A*path search algorithm that introduces a vector cross-product decision value based on the robot energy consumption model in a 2.5D elevation grid map environment. The dynamic weight factor is optimized using the IWOA algorithm based on the dynamic adjustment of uniform population position and inertia weight, which significantly improves the path planning effect and computational efficiency.

The performance testing and path planning experiments of this improved algorithm have been conducted on both the Matlab R2021b simulation environment and the actual orchard operation scenario based on the ROS2 system in this paper. We compare the robustness and effectiveness of our algorithm and those of WOA, LWOA, MWOA, HSWOA, et al. through the average convergence curve of the fitness function under six typical benchmark test functions. Meanwhile, we conduct path planning simulation testing for the A*, standard A*-IWOA, and improved A*-IWOA on six representative scenarios. Especially, we have tested the differences in path planning between 2D and 2.5D grid maps. Finally, to verify the effectiveness of our algorithm, a physical experiment is conducted in a mountainous orchard scene in Gansu province. The results of these experiments effectively demonstrate that this algorithm has significant advantages in computational accuracy, convergence speed, and efficiency. At the same time, the planned path greatly meets the energy consumption and path planning requirements of working robots in unstructured mountain scenes.

Our future research will focus on the following areas:

(1)Improve the algorithm to enhance its path planning effectiveness further.

(2)How to achieve detection and navigation of plant protection robot operation channels under various environmental factors interference.

(3)Implement autonomous navigation operations for plant protection robots based on neuroscience.

Acknowledgements

First of all, I would like to give my heartfelt thanks to all the people who have ever helped me in this paper. This paper was supported by Innovation Fund for College Teachers in Gansu Province No. 2013A-114, Tianshui Normal University Industry Support and Guidance Project No. CYZ2023-05, and Tianshui Normal University Innovation and Entrepreneurship Project No. CXCYJG-JGXM202304JD.

References

[1] Li W, Wang L, Fang D, Li Y, Huang J. 2021. Path planning algorithm combining A* with DWA. Systems Engineering and Electronics 12: 3695-3696.
[2] SoundraPandian KK, Mathur P. 2010. Traversability Assessment of Terrain for Autonomous Robot Navigation. Proc of the Int Multi-Conf of Engineers and Computer Scientists. Hong Kong 1286-1289.
[3] Chen Y, Jiang W, Yang L, Luo Z. 2023. Path planning based on motion constraints for mobile robot. Computer Integrated Manufacturing Systems 4: 1187-1189.
[4] Yuan Y, Ye F, Lai YS, Zhao YT. 2020. Multi AGV Path Planning Combining Load Balancing and A * Algorithm. Computer Engineering and Applications 56(5): 251-256.
[5] Wang DJ. 2012. Path Planning for Indoor Mobile Robots Based on Improved A * Algorithm. Journal of Tsinghua University (Natural Science Edition) 52(8): 1085-1089.
[6] Meng TC, Yang TH, Huang J, Jin WR, Zhang W, Jia YF, Wan KQ, Xiao G, Yang DG, Zhong ZH. 2023. Improved Hybrid A-Star Algorithm for Path Planning in Autonomous Parking System Based on Multi-Stage Dynamic Optimization. International Journal of Automotive Technology 24: 459-468.
[7] Zhai H, Egerstedt M, Zhou H. 2022. Path Exploration in Unknown Environments Using Fokker-Planck Equation on Graph. Journal of Intelligent & Robotic Systems 104: 71.
[8] Manca M, Paternò F, Santoro C. 2021. Remote Monitoring of End-User Created Automations in Field Trials. Journal of Ambient Intelligence and Humanized Computing 13: 5669–5697.
[9] Zakharov K, Saveliev A, Sivchenko O. 2020. Energy-Efficient Path Planning Algorithm on Three-Dimensional Large-Scale Terrain Maps for Mobile Robots. Lecture Notes in Computer Science(ICR 2020), vol 12336.
[10] Lambert P, Godary-Dejean K, Lapierre L, Jaiem L, Crestani D. 2024. Performance Guarantee for Autonomous Robotic Missions using Resource Management: The PANORAMA Approach. Journal of Intelligent & Robotic Systems 110: 52.
[11] Zhang HJ, Zhang YD, Liang RM, Yang TT. 2023. Energy-efficient Path Planning Method for Robots Based on Improved A^* Algorithm. Systems Engineering and Electronics 45(2) : 513-520.
[12] Yin JJ, Dong WL, Liang LH, Xie WD, Xiang ZF. 2019. Optimization Method of Agricultural Robot Path Planning in Complex Environment. Transactions of Chinese Society for Agricultural Machinery 50(5) :17-22.
[13] Jiang YY, Zhang YY. 2022. Path Planning for Improved the A^* algorithm for Searching 8 Domain Nodes. Journal of Electronic Measurement and Instrumentation 36(5) :234-241.
[14] Min HT, Xiong XY, Wang PY, Yu YB. 2021. Autonomous Driving Path Planning Algorithm Based on Improved A^* Algorithm in Unstructured Environment. Proceedings of

Institution of Mechanical Engineers Part D Journal of Automobile Engineering 235(2/3) :513-526.
[15]Shi YT, Chen H, Zhang LX, Sun PF, Pei P, Li DY. 2022. Research on Path Planning of AGV Transfer Robot Based on Improved A* Algorithm. Manufacturing Technology and Machine Tools (5):19-22.
[16]Wu B, Chi X, Zhao C, Zhang W, Lu Y, Jiang D. 2022. Dynamic Path Planning for Forklift AGV Based on Smoothing A* and Improved DWA Hybrid Algorithm. Sensors 22(18):75-78.
[17]Kim HY, Kim HG. 2024. An adaptive continuous–discontinuous approach for the Analysis of Phase Field Fracture Using Mesh Refinement and Coarsening Schemes and Octree-Based Trimmed Hexahedral Meshes. Computational Mechanics. https://doi.org/10.10 07/s00466-024-02472-6.
[18]Saadatzadeh E, Ali Abbaspour R, Chehreghan A. 2023. An Improvement in Smartphone-Based 3D Indoor Positioning Using an Effective Map Matching Method. Journal of Ambient Intelligence and Humanized Computing 14 :13742-13744.
[19]Bays MJ, Wettergren TA, Shin J, Chang S, Ferrari S. 2024. Persistent Schedule Evaluation and Adaptive Re-planning for Maritime Search Tasks. Journal of Intelligent & Robotic Systems 10(65): 18864-18866.
[20]Wang, X., Wang, L.F.S. & Liu, H. 2024. Cross-ownership and managerial delegation under vertical product differentiation. J Econ. https://doi.org/10.1007/s00712-024-00871-0.
[21]Zhai YJ, Cui JH, Meng FB, Xie HW, Hou CY, Li B. 2024. Ship Path Planning Based on Sparse A* Algorithm. Journal of Marine Science and Application. https:// doi.org /10.1007 /s11804-024-00430-5.
[22]Ardestani F, Safdari J, Mallah MH. 2023. Squared-Off Cascades Optimization to Separate Stable Isotopes up to High-Enriched Using Intelligent PSO, WOA, and DA Algorithms. J Eng Phys Thermophy 96: 882–896.
[23]Guo Q, Du X., Zhang Y., Zhou Y. 2021. Three-dimensional Path Planning of UAV Based on Improved Whale Optimization Algorithm. Computer Science 12: 304-311.
[24]Rahimnejad A, Akbari E, Mirjalili S, Andrew Gadsden S, Trojovský P, Trojovská E. 2023. An Improved Hybrid Whale Optimization Algorithm for Global Optimization and Engineering Design Problems. PeerJ Computer Science 11: 1557.
[25]Yang H, Liu S. 2022. Water quality prediction in sea cucumber farming based on a GRU neural network optimized by an improved whale optimization algorithm. PeerJ Computer Science 8:1000.
[26]Li JP, Gong YH, Lu AP, Li PC. 2017. Application of improved particle swarm optimization to numerical function optimization. Journal of Chongqing University 40(5): 95- 103.
[27]Zhou JZ, Lu WW, Sun N, Ye L, Zhang HR, Chen L. 2017. Study on Multi-objective Calibration of Hydrological Model and Optimization Method of Optimal Pareto Solutions. Journal of China Hydrology 37(2): 1-7.
[28]Li N. 2024. Obstacle Avoidance Path Planning for Mobile Robots Based on Convex Optimization.Scientific and technological innovation and application 14(18): 37-40.

[29]Cai ZF, Zhang YS, Liang XZ, Luo SH. 2024. Research on path planning based on improved A* algorithm. Modern information technology 8(10): 51-55.
[30]Zhao Y, Peng Z. 2023. Finite Element Model Updating Based on SGMD and LWOA-ELM. Chinese Journal of Computational Mechanics 2: 255-263.
[31]Niu NP, Zhai DH, Ji HT. 2024. Application of Modified Whale Optimization Algorithm on Trajectory Planning for Mining Inspection Robot. Coal Mine Machinery 45(6): 215-217.
[32]Liang J, Hong Z, Yu S. 2023. Image segmentation model based on improved particle swarm optimization algorithm and genetic mutation. Journal of Computer Applications 6: 1743-1749.
[33] Saha N, Sahoo SK, Rout B, Panda S, Panda G, Sahoo DK. 2022. Solar PV-Powered SRM Drive and its Speed Control and Torque Ripple Minimization. Sustainable Energy and Technological Advancements 3: 293-306.
[34] Cheng H, Wang M, Wang L, Zhang X. 2022. Whale Algorithm Based on Coupled Center Wander and Double Weight Factors and Its Applications. Computer Engineering and Applications 13: 74-84.
[35] Huang X, Lu Y, Shen L, Lin B. 2023. Multi-objective Constrained Optimization Problem Solving Based on Particle Swarm Optimization and Gray Wolf Hybrid Algorithm. Journal of Chinese Computer Systems 2: 288-299.
[36]Ren L, Lai HC, Chen QZ, Wang X. 2013. Based on improved K-means clustering cotton image segmentation algorithm. Computer Engineering and Design 34(5): 1772-1776.
[37]Akay B, Karaboga D. 2010. Artificial Bee Colony Algorithm for Large-Scale Problems and Engineering Design Optimization. Journal of Intelligent Manufacturing 23:1001-1014.
[38]Akyol S, Alatas B. 2020. Sentiment classification within online social media using whale optimization algorithm and social impact theory based optimization. Physica A: Statistical Mechanics and its Applications 540:123094.
[39]Al-Dabbagh RD, Kinsheel A, Mekhilef S, Baba MS, Shamshirband S. 2014. System identification and control of robot manipulator based on fuzzy adaptive differential evolution algorithm. Advances in Engineering Software 78:60-66.
[40]Aragón VS, Esquivel SC, Coello CAC. 2010. A modified version of a T-Cell Algorithm for constrained optimization problems. International Journal for Numerical Methods in Engineering, 351-378.

Figure 1

Front wheel differential drive Ackermann steering robot coordinate system.

(a) 2D schematic operation diagram; (b)3D space schematic operation diagram.

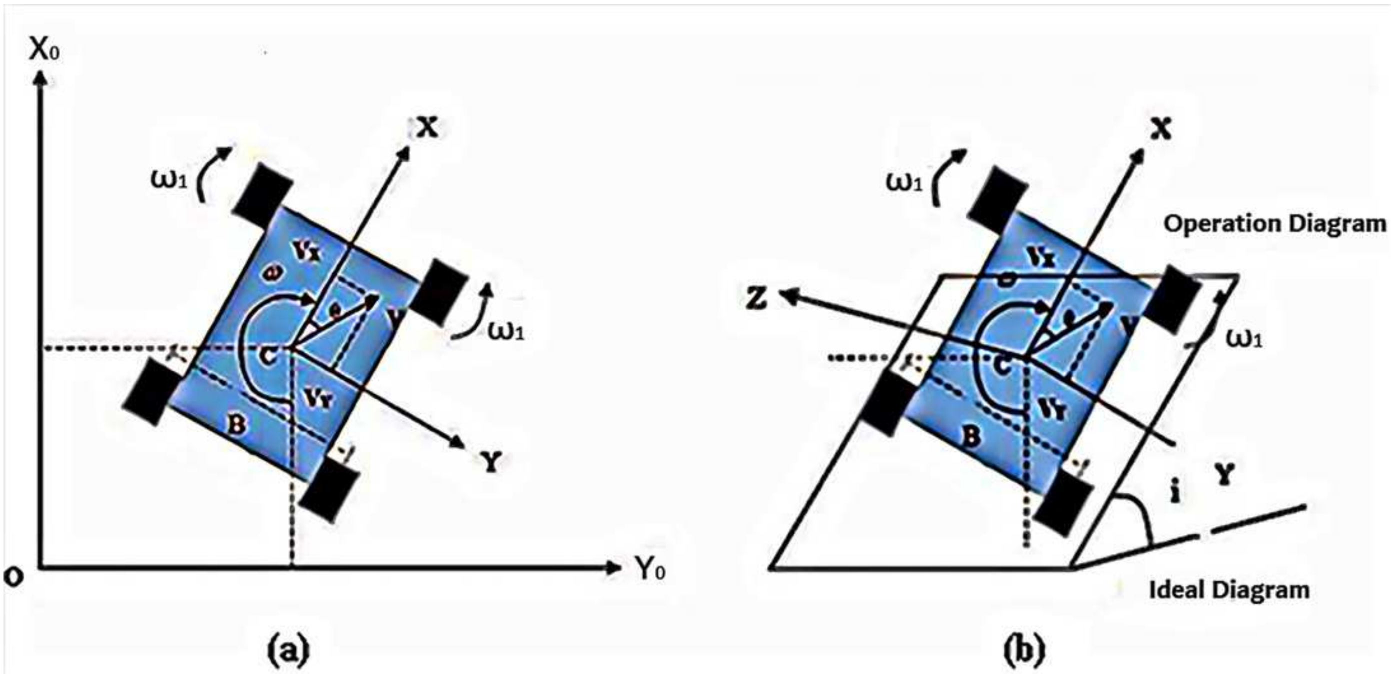

Figure 2

Path planning results comparison of three distance functions.

(a) Non-obstacle situation; (b)Obstacle situation.

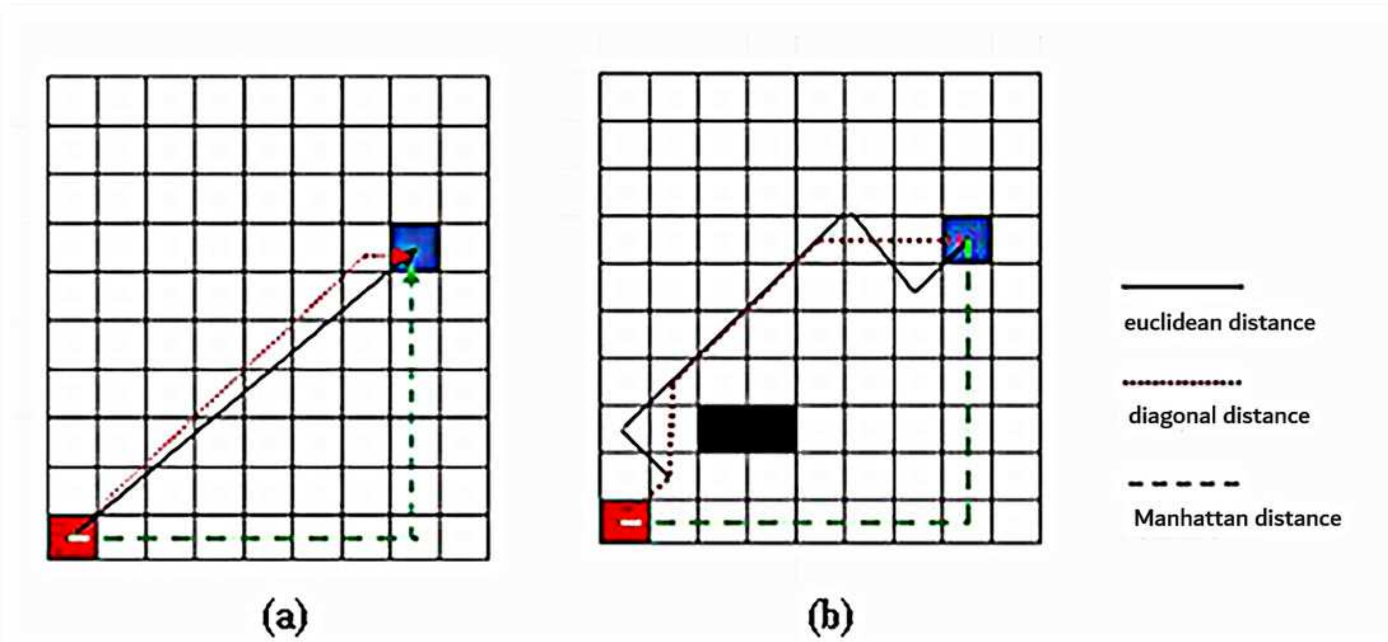

Figure 3

2.5D elevation grid map.

(a) Vertical height of mountain orchard ground; (b) 2D grid map

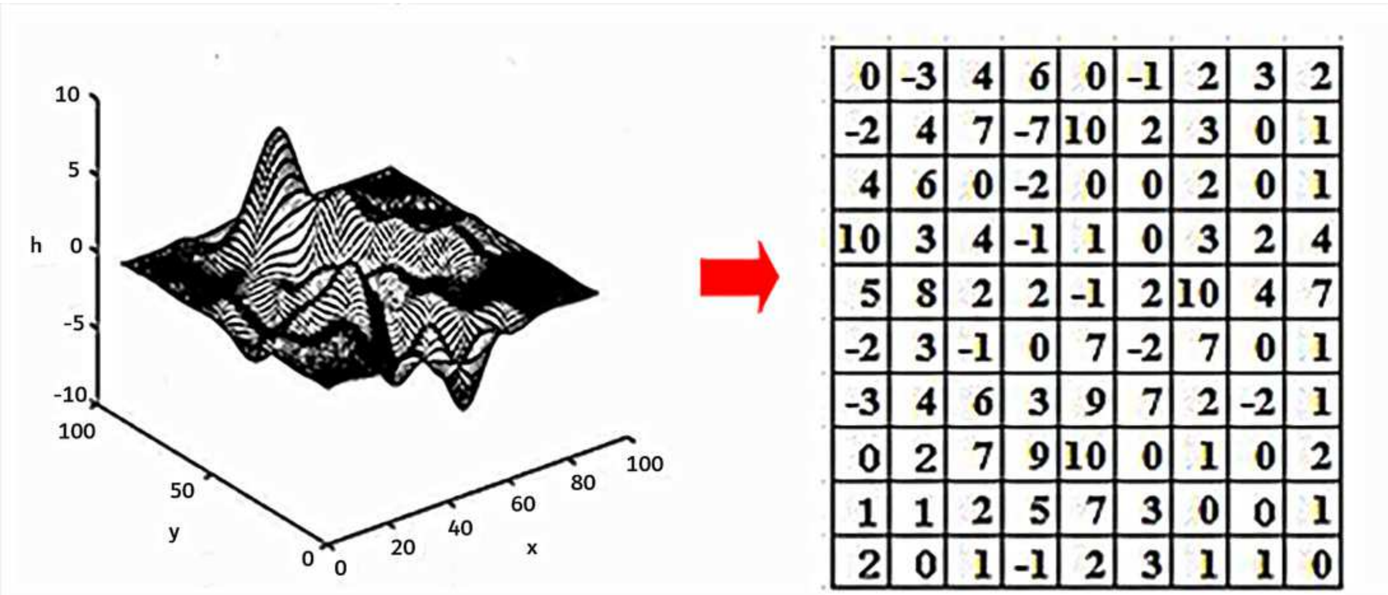

Figure 4

Definition of the cross product.

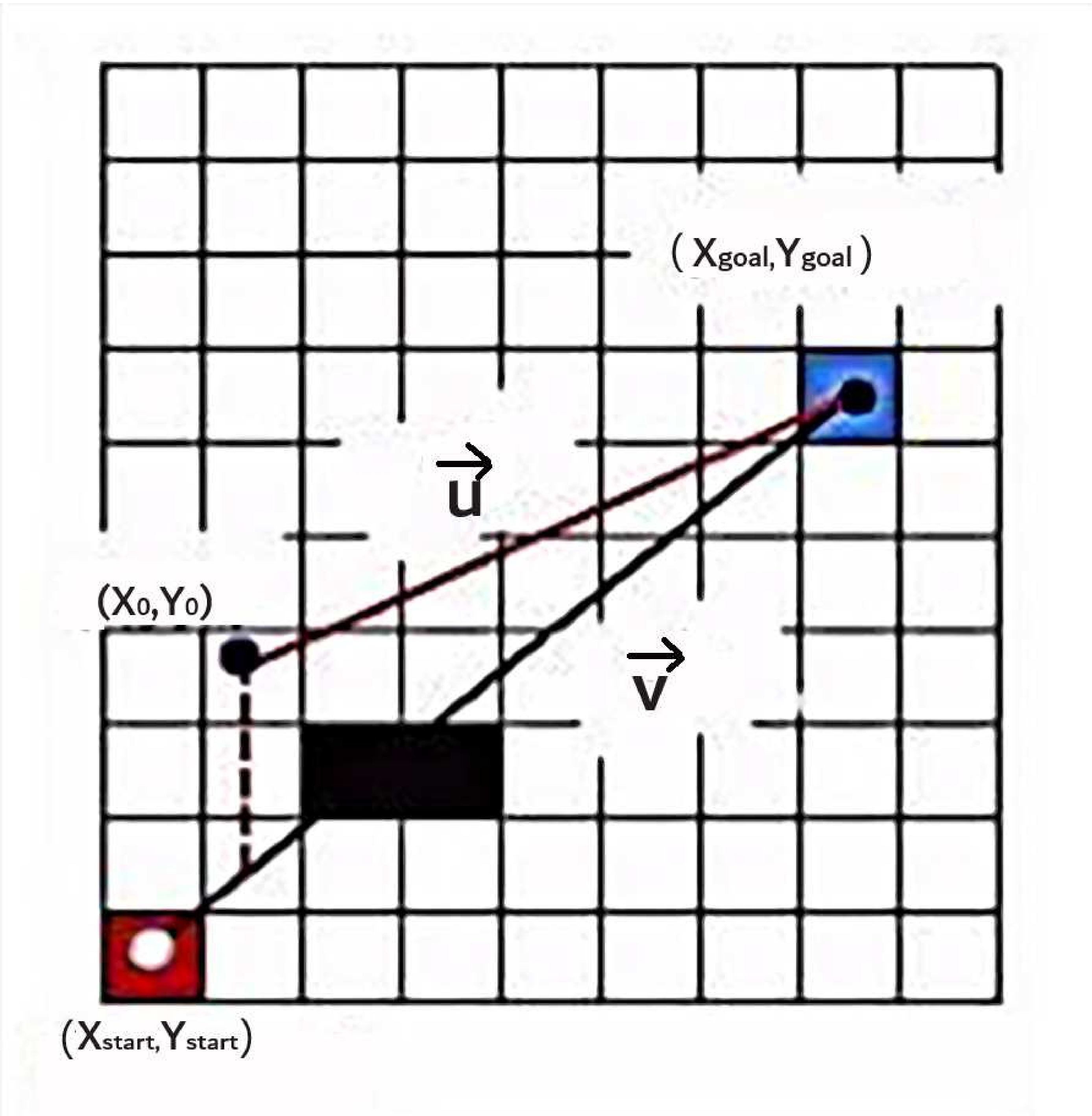

Figure 5

The path of fixed p-factor cross product.

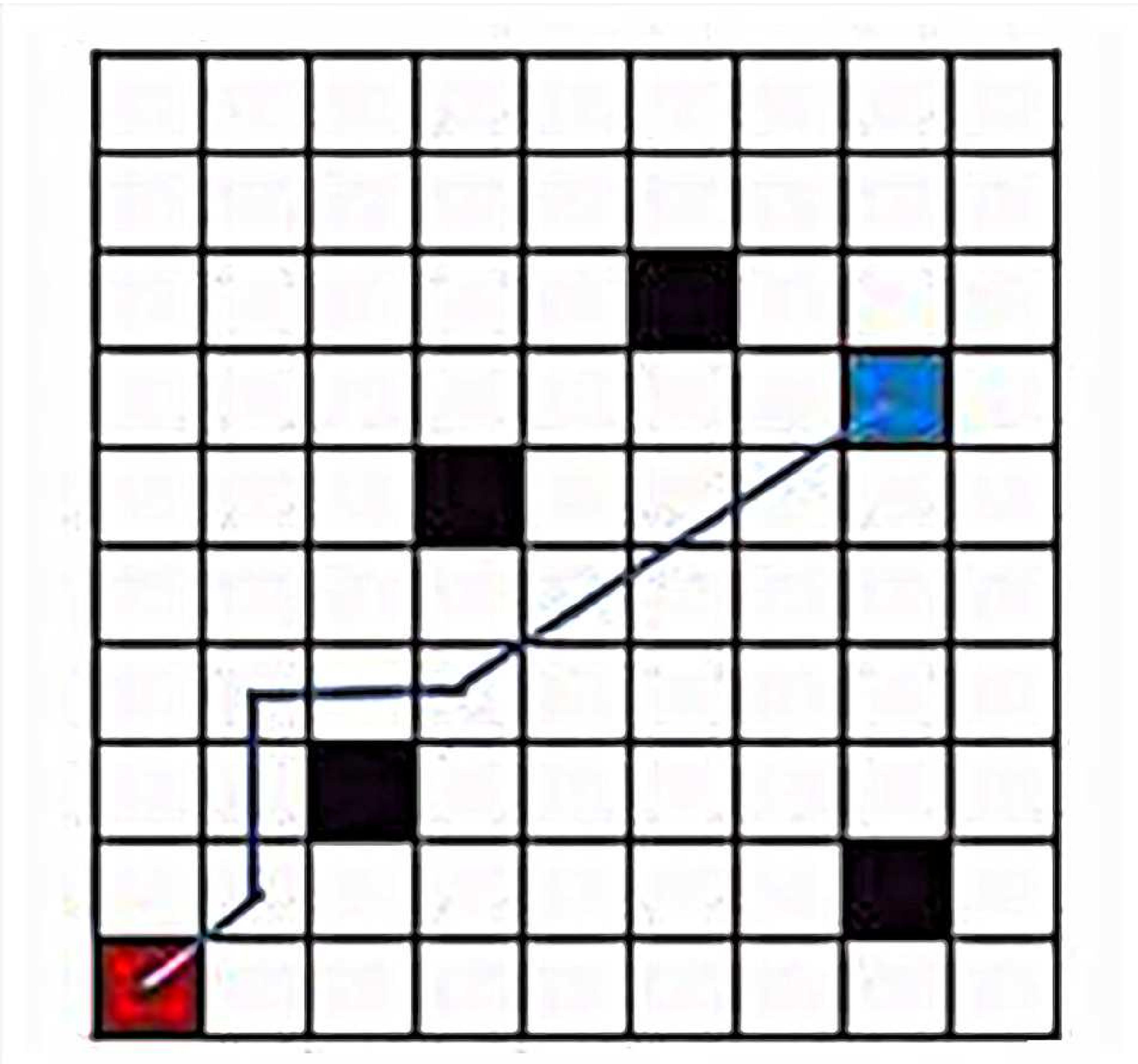

Figure 6

Schematic diagram of the operation trajectory.

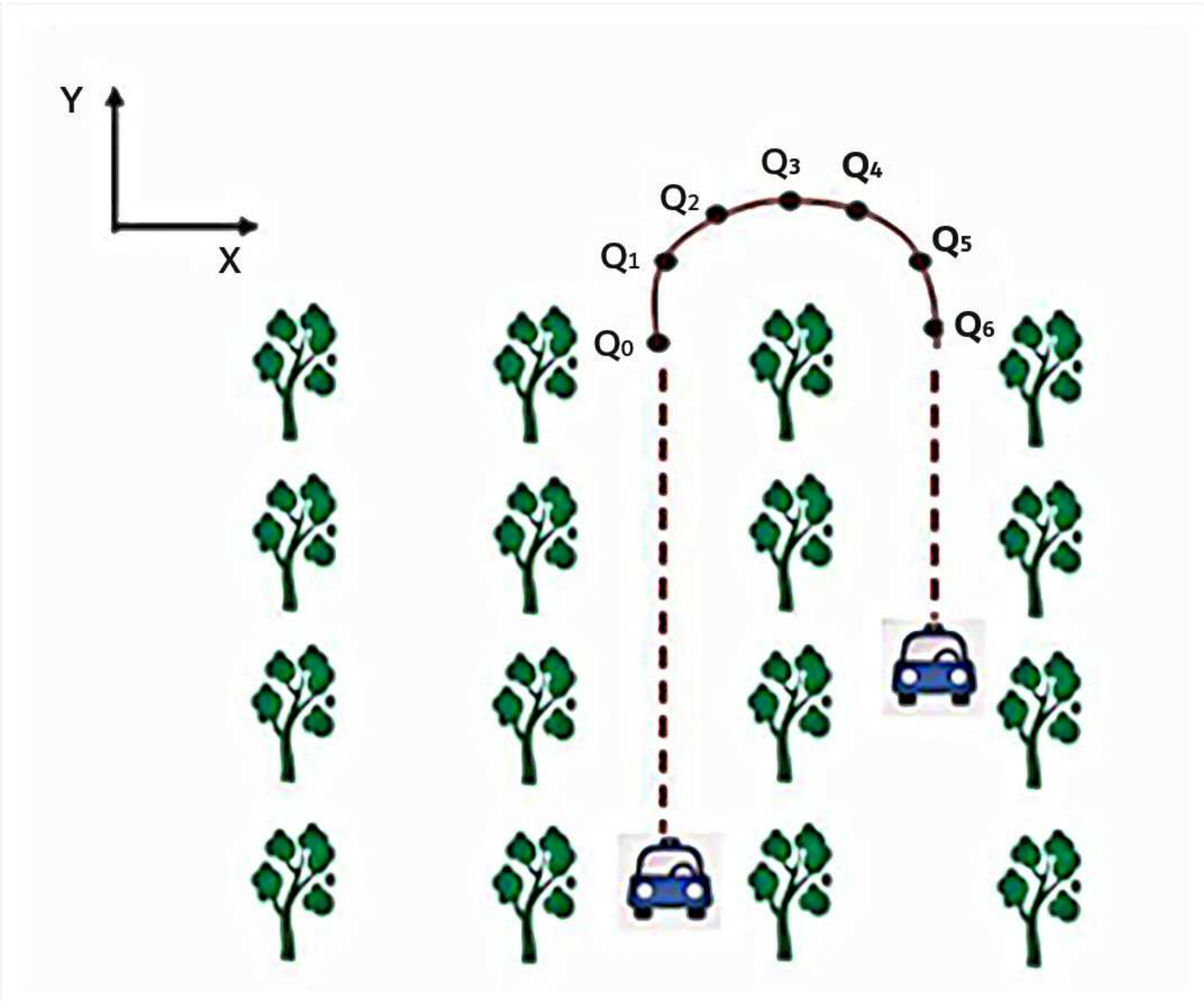

Figure 7

IWOA multi-objective optimization process based on optimal selection.

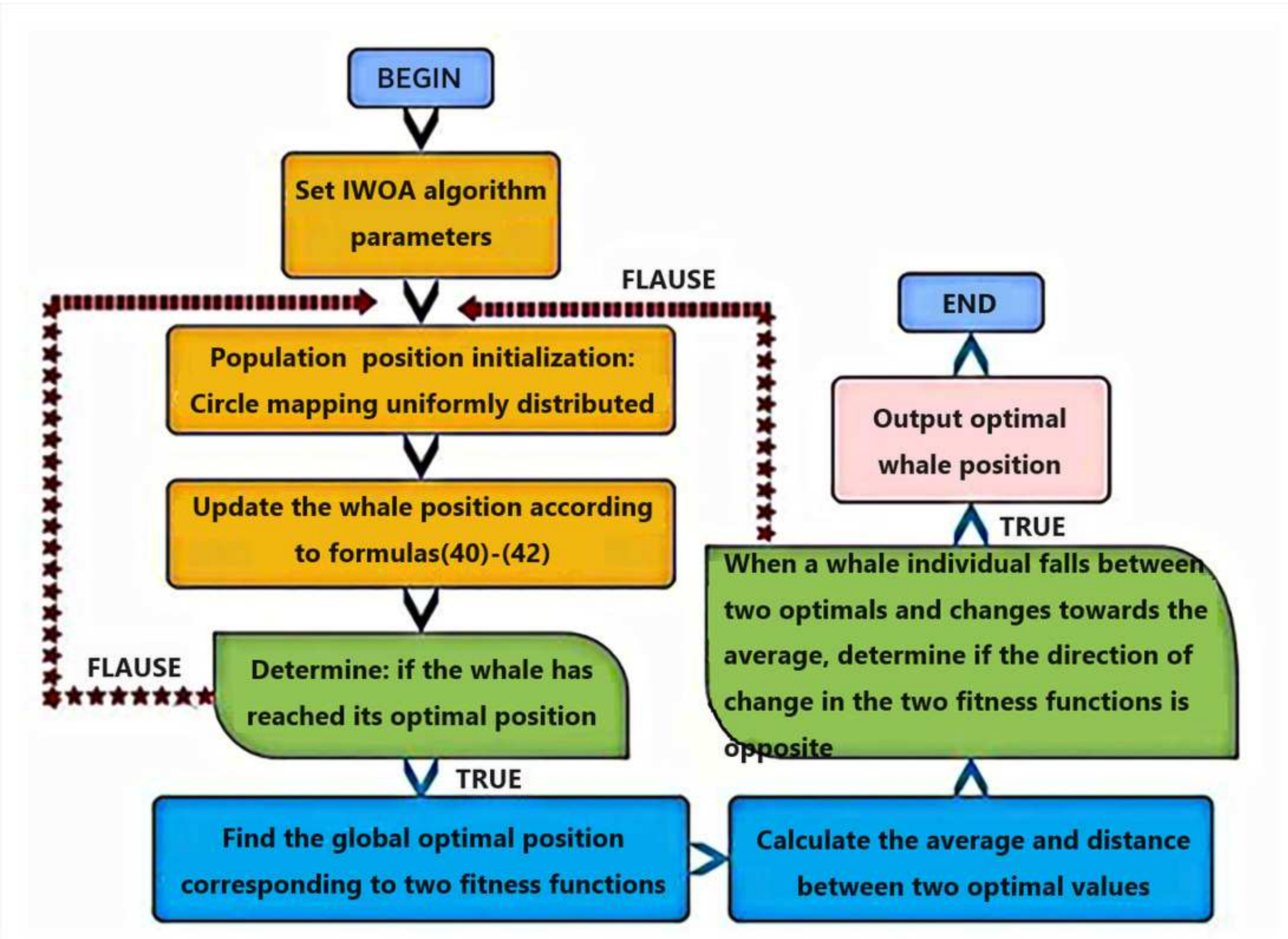

Figure 8

Structure of wheeled plant protection robot.

1. 16 line LiDAR; 2. GNSS navigation system; 3. lithium battery; 4. chassis controller.

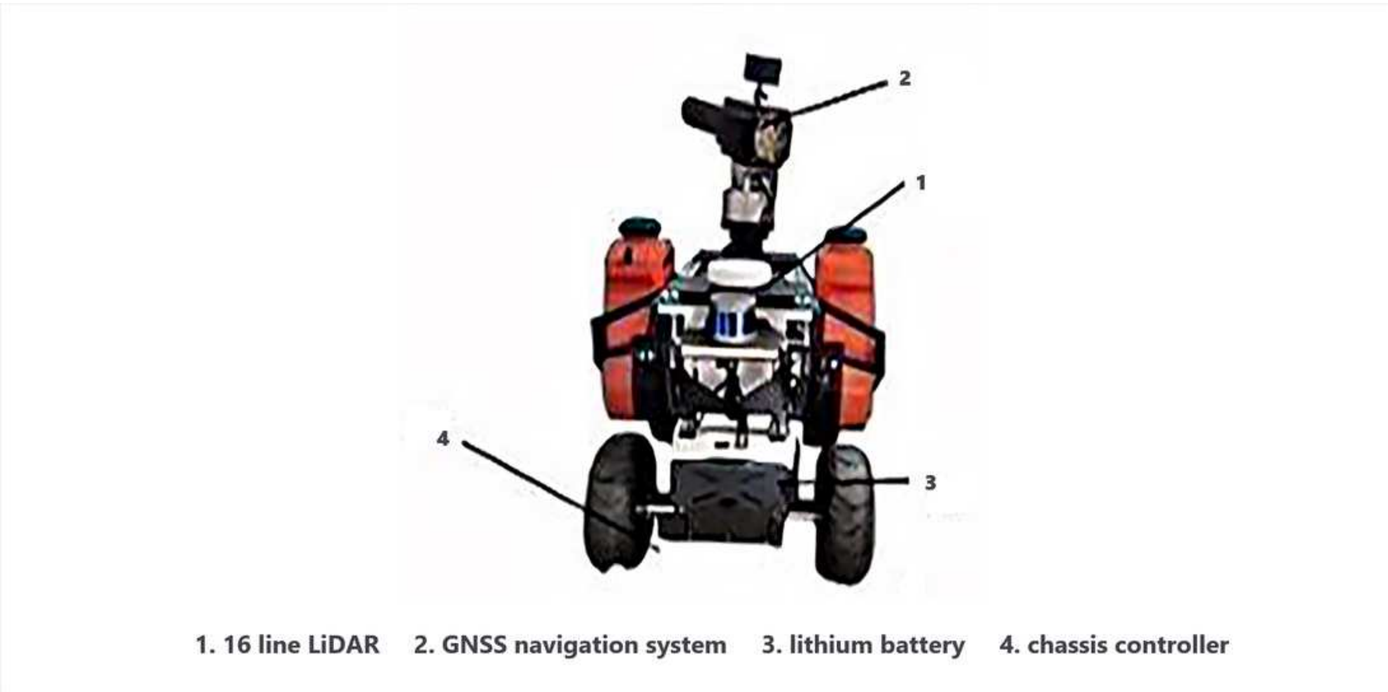

Figure 9

Average convergence curve of fitness of test function.

(a) f_1 curves (b) f_5 curves; (c) f_8 curves; (d) f_{13} curves; (e) f_{15} curves; (f) f_{17} curves

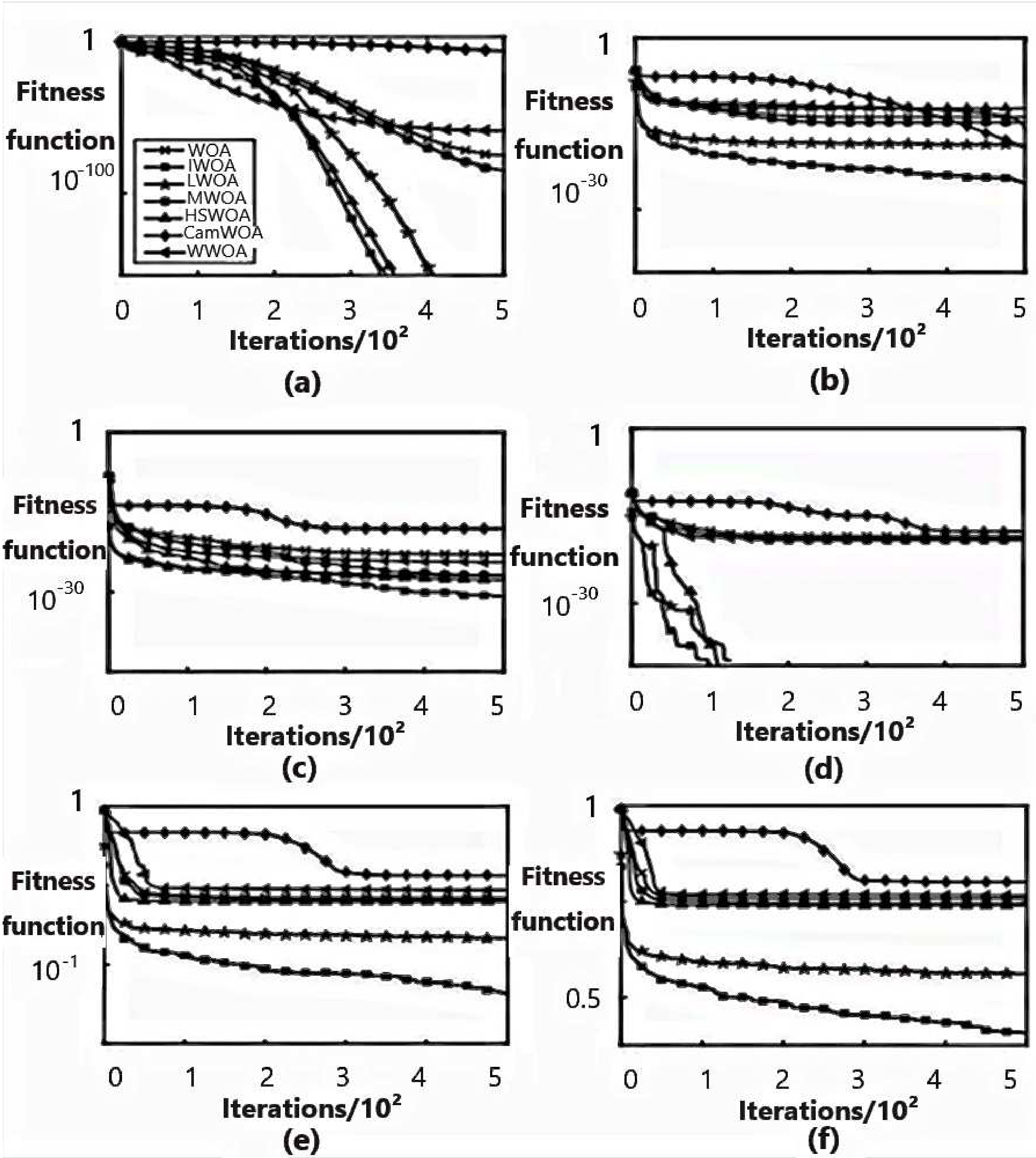
1
Fitness function
10^{-100}
WOA
IWOA
LWOA
MWOA
HSWOA
CamWOA
WWOA
0 1 2 3 4 5
Iterations/10^2
(a)
1
Fitness function
10^{-30}
0 1 2 3 4 5
Iterations/10^2
(b)
1
Fitness function
10^{-30}
0 1 2 3 4 5
Iterations/10^2
(c)
1
Fitness function
10^{-30}
0 1 2 3 4 5
Iterations/10^2
(d)
1
Fitness function
10^{-1}
0 1 2 3 4 5
Iterations/10^2
(e)
1
Fitness function
0.5
0 1 2 3 4 5
Iterations/10^2
(f)

Figure 10

The path planning test results.

(a) Scene 1; (b) Scene 2; (c) Scene 3; (d) Scene 4; (e) Scene 5; (f) Scene 6.

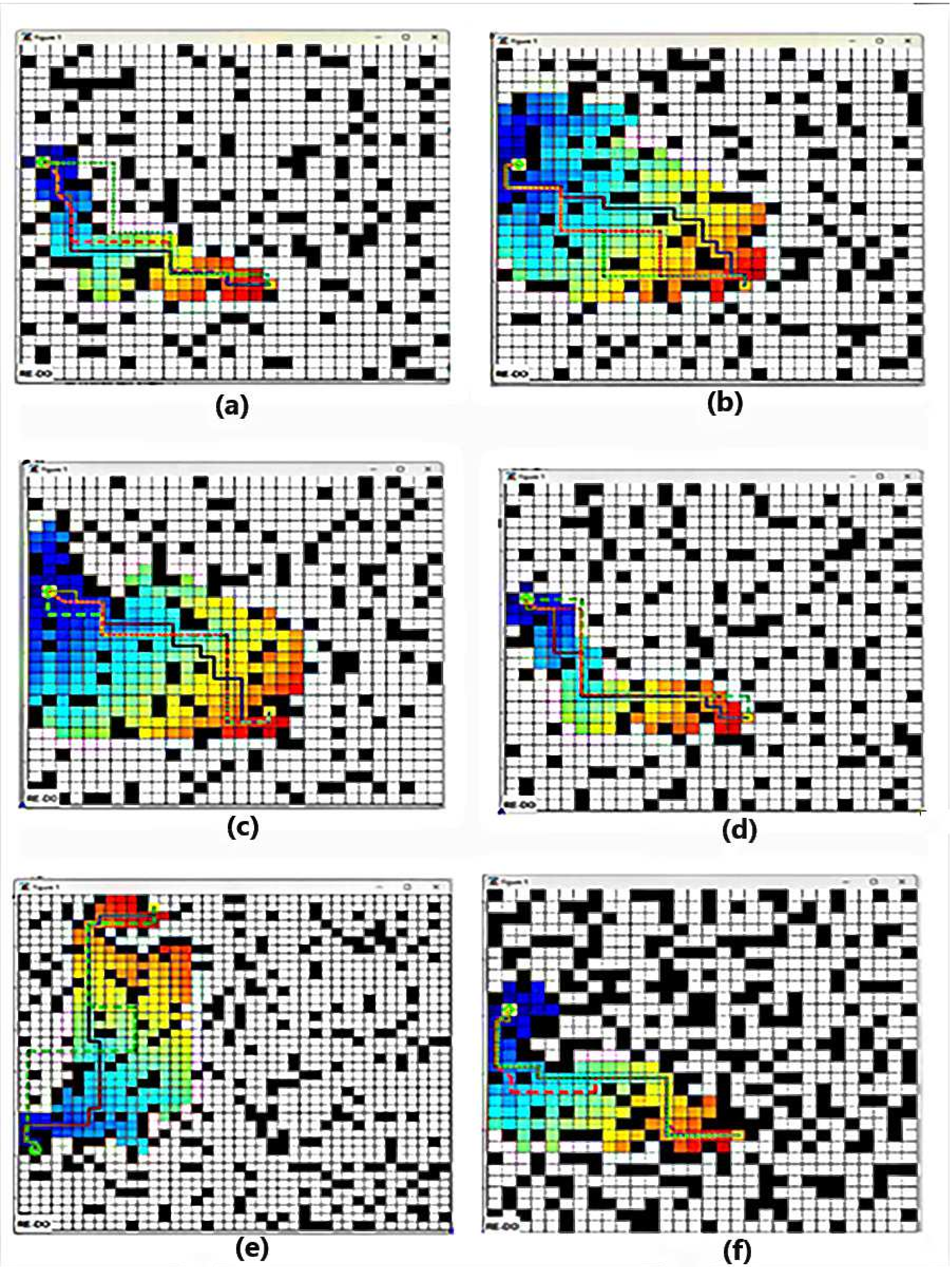

(a) (b) (c) (d) (e) (f)

Figure 11

Comparison of planning effects on 2D and 2.5D maps.

(a)2D map planned path; (b) 2.5D map planned path.

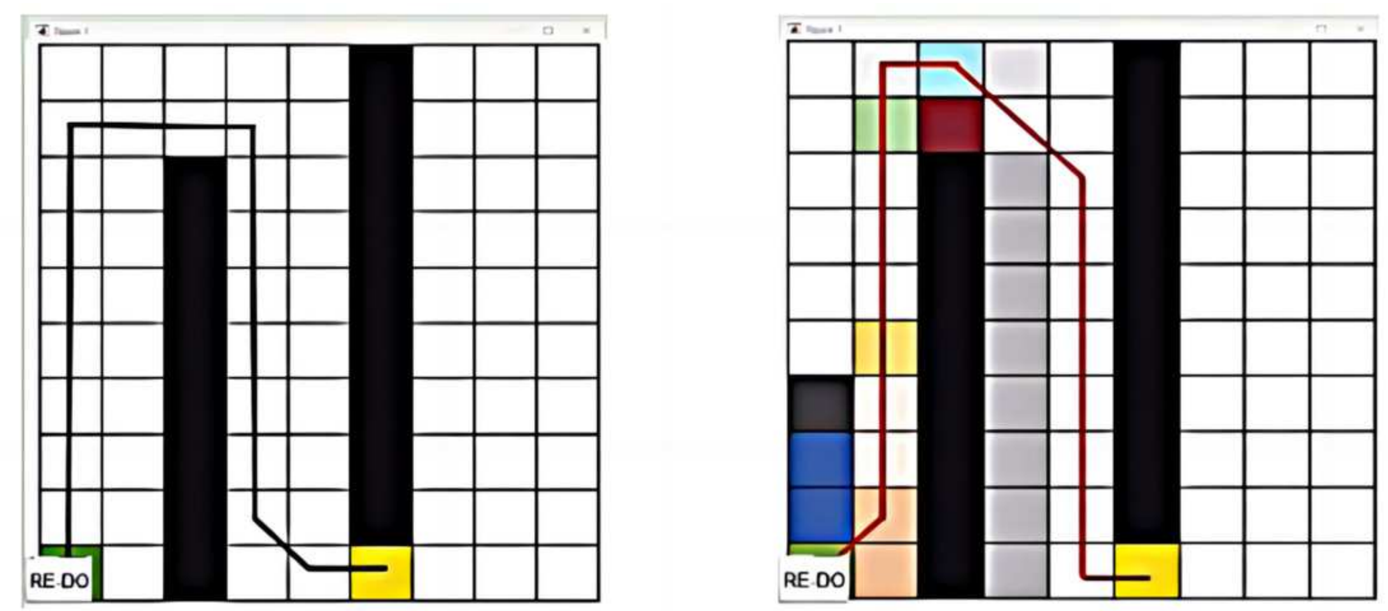

Figure 12

Real environment.

Figure 13

Real orchard point clouds.

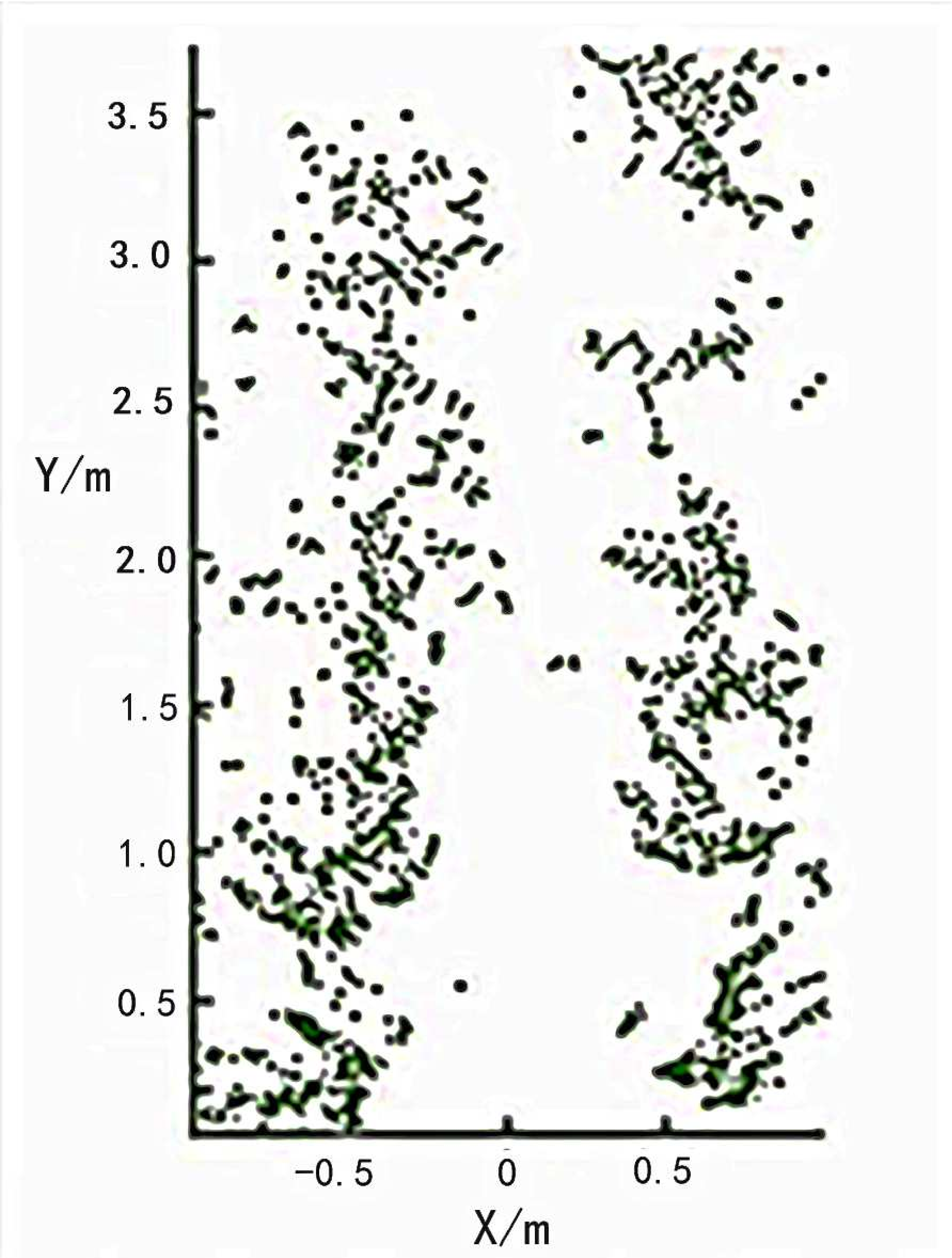
3.5
3.0
2.5
Y/m
2.0
1.5
1.0
0.5
-0.5
0
0.5
X/m

Figure 14

Comparison of three algorithms for path planning in real orchard.

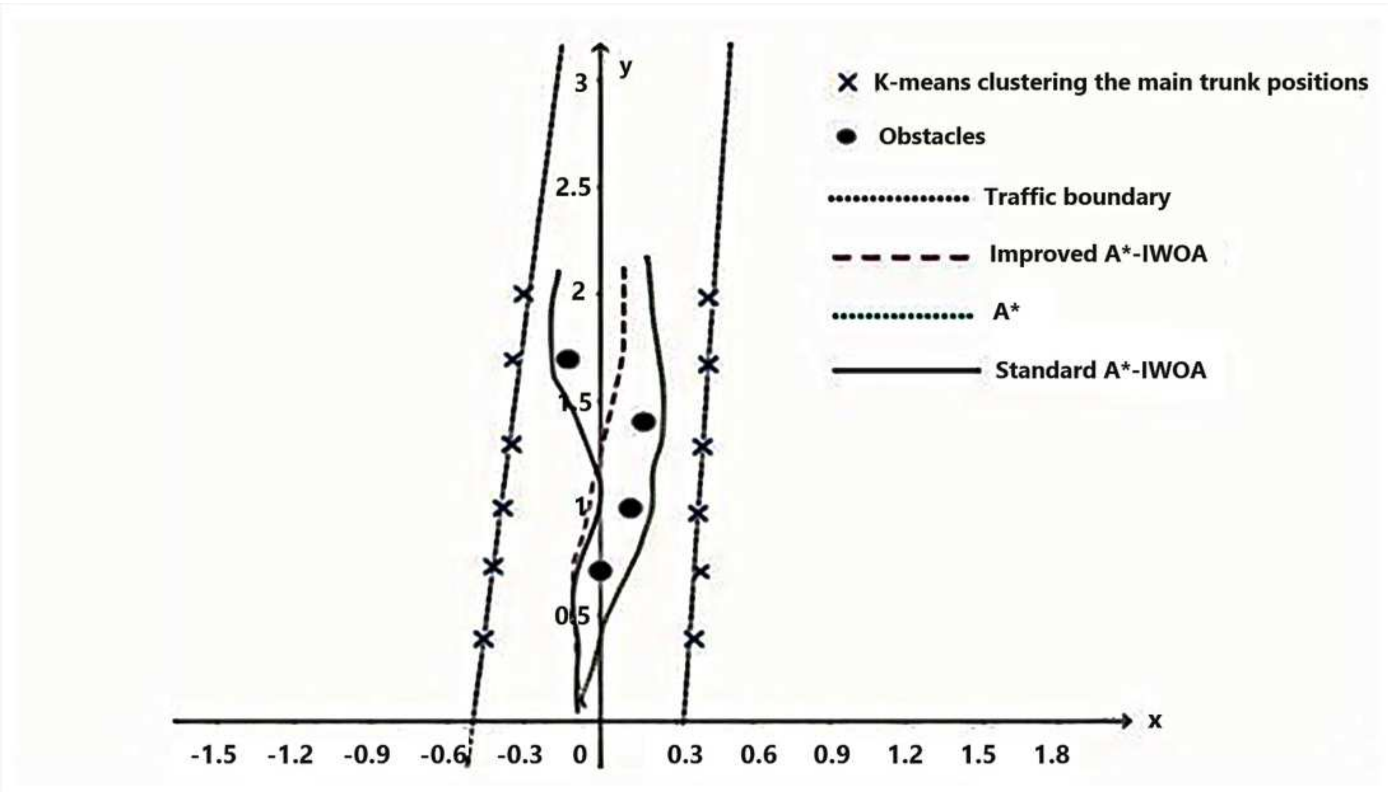

Table 1(on next page)

Improved IWOA algorithm pseudo code.

Table 1. Improved IWOA algorithm pseudo code.

01	Set population size as N, maximum number of iterations as T
02	According to formula (38), initialize the population position following the Circle map and calculate the fitness of each individual to determine the optimal individual position
03	Calculate the inertia factor according to formula (39), and update A and C according to formulas (41) to (42)
04	While(t<T)
05	for each individual
06	Calculation parameters a,A,C,l,p
07	if p<0.5
08	if $\lvert A \rvert < 1$
09	Update individual position using formula (40-1)
10	else
11	Update individual position using formula (40-2)
12	end if
13	else
14	Update individual position using formula (40-3)
15	end if
16	end for
17	Recalculate individual fitness according to formula (29) boundary constraint processing
18	Update Best Individual
19	t=t+1
20	end while
21	Output global optimal solution and optimal fitness
22	end

Table 2(on next page)

List of benchmark function parameters.

Table 2. List of benchmark function parameters.

Benchmark Functions	***Dimension***	***Range***	***Theoretical Minimum Value***
$f_1(x) = \sum_{i=1}^{n} x_i^2$	30	[-100,100]	0
$f_5(x) = \sum_{i=1}^{n-1}[100(x_{i+1} - x_i^2)^2 + (x_i - 1)^2]$	30	[-30,30]	0
$f_8(x) = \sum_{i=1}^{n} -x_i sin(\sqrt{\lvert x_i \rvert})$	30	[-500,500]	0
$f_{13}(x) = 0.1$ $\{sin^2(3\pi x_1) + \sum_{i=1}^{n}(x_i - 1)^2[1 + sin^2(3\pi x_i + 1) + (x_i$	30	[-50,50]	0
$f_{15}(x) = \sum_{i=1}^{11}[a_i - \frac{x_1(b_i^2 + b_1 x_2)}{b_i^2 + b_1 x_3 + x_4}]^2$	4	[-5,5]	0.1484
$f_{17}(x) = (x_2 - \frac{5.1}{4\pi^2}x_1^2 + \frac{5}{\pi}x_1 - 6)^2 + 10(1 - \frac{1}{8\pi})cosx_i$ $+ 10$	2	[-5,5]	0.3

Table 3 (on next page)

Test results data.

Table 3. Test results data.

Function	*Algorithms*	*Optimal*	*Worst*	*Average*	*Standard*	*Consuming/s*
f_1	Improved IWOA	0.00e+00	0.00e+00	0.00e+00	0.00e+00	1.0233
	WOA	1.47e-178	3.01e-161	2.35e-173	4.38e-170	1.9038
	LWOA	0.89e-121	2.75e-149	1.78e-151	8.41e-201	1.7544
	MWOA	1.02e-130	7.88e-171	6.07e-154	1.34e-149	1.7068
	HSWOA	1.02e-131	2.00e-161	2.32e-158	5.18e-180	1.2331
	CamWOA	6.67e-118	3.01e-152	8.35e-133	3.47e-170	1.1138
	WWOA	3.47e-150	5.71e-131	2.39e-143	7.33e-172	1.1189
f_{13}	Improved IWOA	0.00e+00	0.00e+00	0.00e+00	0.00e+00	0.8724
	WOA	1.32e-201	3.81e-191	7.55e-193	3.18e-200	1.2008
	LWOA	0.78e-181	2.21e-169	1.18e-171	2.40e-206	1.0044
	MWOA	1.41e-200	7.01e-181	9.11e-194	1.34e-221	1.0068
	HSWOA	3.01e-191	7.36e-164	2.31e-178	5.10e-200	1.2071
	CamWOA	8.67e-218	3.71e-152	8.31e-183	3.47e-190	1.1130
	WWOA	3.41e-190	6.93e-211	2.32e-203	7.33e-221	0.9189
f_{15}	Improved IWOA	0.20e+00	0.09e+00	0.10e+00	0.03e-02	0.9331
	WOA	1.32e+00	7.12e+00	1.39e+00	1.18e-110	1.7328
	LWOA	0.73e+00	0.99e+00	0.80e+00	2.40e-106	1.1114
	MWOA	0.71e+00	1.21e+00	1.01e+00	1.14e-121	1.2260
	HSWOA	0.43e+00	0.93e+00	0.99e+00	2.91e-100	1.2099
	CamWOA	0.67e+00	1.91e+00	1.45e+00	1.47e-090	1.9130
	WWOA	0.49e+00	0.88e+00	0.78e+00	5.49e-121	1.1181

Table 4(on next page)

The kinematic parameters of the robot.

Table 4. The kinematic parameters of the robot.

Maximum Limit	***Value***
Maximum linear speed	1.5
Maximum angular velocity	0.8
Maximum angular acceleration	0.3
Maximum linear acceleration	0.4

Table 5 (on next page)

The initial parameter settings of improved A*-IWOA.

Table 5. The initial parameter settings of improved A*-IWOA.

Initial Parameters	*Value*
Grid environment	20×20/30×30
Starting point coordinates	35
End point coordinates	285
Initial population size	30
Maximum Number Of Iterations	500

Table 6(on next page)

Road planning result data for 6 scenes.

Table 6. Road planning result data for 6 scenes.

Scenes	*Algorithms*	*Total distance*	*Turning points*	*Time/s*
1	A*	33.0	8	1.30
	standard A*-IWOA	33.4	9	1.21
	improved A*-IWOA	27.0	5	0.79
2	A*	30.1	11	1.27
	standard A*-IWOA	30.3	11	1.20
	improved A*-IWOA	29.0	8	0.88
3	A*	37.4	13	1.28
	standard A*-IWOA	34.2	10	1.27
	improved A*-IWOA	30.0	6	0.81
4	A*	33.4	9	1.29
	standard A*-IWOA	30.0	7	1.20
	improved A*-IWOA	27.0	3	0.96
5	A*	30.0	11	1.14
	standard A*-IWOA	30.0	10	1.10
	improved A*-IWOA	28.4	8	0.84
6	A*	31.0	8	0.77
	standard A*-IWOA	30.0	9	0.80
	improved A*-IWOA	29.0	6	0.79